NASA TECHNICAL NOTE

NASA TN D-4198

NASA TN D-4198

DYNAMIC FLIGHT BEHAVIOR OF A BALLASTED SPHERE AT MACH NUMBERS FROM 0.4 TO 14.5

by Barbara J. Short

Ames Research Center

Moffett Field, Calif.

NATIONAL AERONAUTICS AND SPACE ADMINISTRATION • WASHINGTON, D. C. • OCTOBER 1967

NASA TN D-4198

DYNAMIC FLIGHT BEHAVIOR OF A BALLASTED SPHERE AT MACH NUMBERS FROM 0.4 TO 14.5

By Barbara J. Short

Ames Research Center
Moffett Field, Calif.

NATIONAL AERONAUTICS AND SPACE ADMINISTRATION

For sale by the Clearinghouse for Federal Scientific and Technical Information
Springfield, Virginia 22151 – CFSTI price $3.00

DYNAMIC FLIGHT BEHAVIOR OF A BALLASTED SPHERE AT MACH NUMBERS FROM 0.4 TO 14.5

By Barbara J. Short

Ames Research Center

SUMMARY

A ballasted sphere with a static margin of 14 percent of the diameter was tested at Mach numbers from 0.4 to 14.5 and Reynolds numbers between 0.4×10^6 and 1.6×10^6. It was found to be dynamically unstable. At supersonic and hypersonic speeds the oscillatory motions were orderly and the static stability was predictable. At low speeds the angular motions were erratic and so were the characteristics of the boundary layer as it separated from the body to form the wake.

INTRODUCTION

The aerodynamics of spheres has been of great academic interest for many years. Spheres would be of practical interest for some flight missions if they could be made to fly smoothly and stably. Seiff and Peterson discussed the advantages of spherical geometry for an atmosphere probe to be flown into the atmospheres of nearby planets (refs. 1-3). On-board measurements including those of pressure, temperature, and three components of acceleration would be used to deduce the atmospheric structure. The unique advantage of the sphere is that its drag coefficient is independent of attitude and is insensitive to flight conditions at high speeds (refs. 4-7). Practical considerations, such as communication of data to either Earth or a relay station (ref. 8), require that the probe be statically and dynamically stable about a known axis. To this end an experimental program was undertaken to determine the flight characteristics of a ballasted sphere with its center of gravity located 0.14 d off center.

SYMBOLS

A	cross-section area of sphere
C_D	drag coefficient, $\frac{\text{drag}}{q_\infty A}$
C_L	lift coefficient, $\frac{\text{lift}}{q_\infty A}$

C_{L_α} lift-curve slope, $\left(\frac{\partial C_L}{\partial \alpha}\right)_{\alpha \to 0}$

C_m pitching-moment coefficient, $\frac{\text{pitching moment}}{q_\infty Ad}$

C_{m_α} pitching-moment-curve slope, $\left(\frac{\partial C_m}{\partial \alpha}\right)_{\alpha \to 0}$

$C_{m_q} + C_{m_{\dot{\alpha}}}$ damping-in-pitch derivative, $\left[\frac{\partial C_m}{\partial q(d/V)}\right]_{q \to 0} + \left[\frac{\partial C_m}{\partial \dot{\alpha}(d/V)}\right]_{\dot{\alpha} \to 0}$

d maximum diameter of sphere

I_x moment of inertia about the longitudinal axis through the center of gravity

I_y moment of inertia about the transverse axis through the center of gravity

M Mach number

q angular pitching velocity

q_∞ free-stream dynamic pressure

R Reynolds number based on d and free-stream air properties

V velocity along the flight path

$\overline{x}$ static margin, distance along the longitudinal axis between the center of gravity and the center of volume, divided by d

α angle of attack (angle between model axis and resultant wind direction projected onto the vertical plane)

$\dot{\alpha}$ first derivative of α with respect to time

β angle of sideslip (angle between model axis and resultant wind direction projected onto the horizontal plane)

γ inclination of the edge of the near wake with respect to the flight direction (see sketch p. 6)

δ polar angle from direction of flight to flow transition in the wake (see sketch p. 6)

θ polar angle from direction of flight to boundary-layer-flow separation (see sketch p. 6)

ξ dynamic-stability parameter, $C_D - C_{L_\alpha} + (C_{m_q} + C_{m_{\dot{\alpha}}})(d/\sigma)^2$

σ radius of gyration about the transverse axis through the center of gravity

EXPERIMENTAL PROCEDURE

Ballasted spheres were gun-launched into still air past a series of spark shadowgraph stations which recorded time-distance histories and attitude histories of the sphere in free flight.

Models

Most of the spheres were made of 7075 T6 aluminum and ballasted with a tungsten alloy (Mallory 3000) to position the center of gravity 0.14 d ahead of the center of volume with an inertia ratio, I_y/I_x, of 1.2 (fig. 1(a)). In order to determine the effect of mass distribution on the oscillatory motions of the sphere in free flight a few tests were conducted with nylon spheres ballasted with SAE 4340 steel (fig. 1(b)). A static margin of 14 percent of the diameter was maintained while the inertia ratio was reduced from 1.2 to 0.8.

Two sizes of spheres were used, 0.4-inch and 1.6-inch diameter. A spike on the axis at the base was used to measure the attitude of the sphere from the shadowgraphs.

Test Conditions and Equipment

The Mach number and Reynolds number regimes of this investigation are indicated by the curves in figure 2. For the tests in the hypersonic regime, the small spheres (0.4-inch diameter) were fired through still air at approximately one-fourth atmospheric pressure. These spheres were launched from a deformable-piston, light-gas gun in the Ames Prototype Hypervelocity Free-Flight Facility. The test section of this facility is 40 feet long with 11 spark shadowgraph stations spaced 4 feet apart.

For the tests at a nominal Mach number of 5 the small spheres were fired through still air at 1 atmosphere pressure. These spheres were launched from a 50-caliber smooth-bore gun in the Ames Supersonic Free-Flight Wind Tunnel (ref. 9). The test section of this facility was 24 feet long with 9 spark shadowgraph stations spaced 3 feet apart.

The large spheres (1.6-inch diameter) were fired at low supersonic and subsonic speeds through still air at 1 atmosphere pressure. These spheres were launched from a 57-mm smooth-bore gun in the Ames Pressurized Ballistic Range. The test section of this facility is 203 feet long with 24 spark shadowgraph stations spaced from 7 to 14 feet apart.

DATA REDUCTION

The time-distance histories were used to determine the drag of the sphere in free flight by the method described in reference 10. The drag coefficient, C_D, was computed from the measured deceleration of the sphere.

The attitude histories were used to determine the stability parameters by the method described in reference 11. With this method the pitching-moment-curve slope, C_{m_α}, is computed from the wavelength of oscillation, and the dynamic-stability parameter, ξ, is determined from the growth or decay of the amplitude of oscillation.

Illustrations of the types of motions encountered in the present tests, as viewed in the α-β plane, are shown in figure 3. The solid curves in this figure and all subsequent figures showing angular motions were obtained from a least-squares fit to the data points using the analysis described in reference 11. In the hypersonic and supersonic regimes, the angular motions were nearly planar oscillations which slowly grew in amplitude, as seen in figures 3(a), (b), and (c). In the low supersonic and subsonic regimes, the angular motions of a few flights were regular enough to allow analysis for stability results (fig. 3(d)). The motions of most of the flights in this regime, however, were very erratic with no defined wavelength of oscillation or rate of growth of amplitude, as seen in figure 3(e). The dashed curve represents a hand fairing through the data points. The fairing is a cross plot of hand fairings of α and β versus flight-path distance. The only aerodynamic parameter which could be derived from motions such as shown in figure 3(e) was the drag coefficient.

Ballistic-range data at subsonic speeds are compared with some unpublished flight data in figure 4. The motion seen in figure 4(b) was obtained by Messrs. S. C. Sommer and A. G. Boissevain of Ames, who installed a movie camera internally at the stagnation point of a 2-foot-diameter ballasted sphere which was dropped from an aircraft at 40,000 feet altitude. The angular motion was deduced from the film with the aid of a topographical map. As can be seen, the kind of erratic motion obtained in the present investigation is by no means restricted to the ballistic range.

RESULTS AND DISCUSSION

Angular Motions

To investigate the effect of mass distribution on the oscillatory motions, a few tests were conducted with spheres with an inertia ratio, I_Y/I_X, less than 1 (fig. 1(b)). The angular motion seen in figure 5(a) was obtained with one of these spheres at a Mach number of 1.5. A comparison of this motion with that shown in figure 5(b) at the same test conditions indicated that the sphere with the low inertia ratio would exhibit a slowly precessing elliptical motion more amenable to analysis for stability results. However,

two tests at transonic speeds showed that two spheres with different inertia ratios experienced very similar erratic motions, as seen in figures 5(c) and (d). The mass distribution of the spheres does not seem to be a controlling factor on the type of motion. The characteristics of the boundary layer as it separated from these two bodies to form the wake will be discussed in the following section.

Boundary-Layer-Flow Parameters

The shadowgraphs showed that the two spheres with different inertia ratios but similar erratic angular motions at transonic speeds also had very similar asymmetric boundary-layer separation patterns which fluctuated with time. Shadowgraph prints of these two spheres at $M = 1.0$ are shown in figure 6. The flight direction is within 1° of the horizontal reference wires in the shadowgraphs. Both shadowgraphs show that laminar boundary-layer separation occurs at about 85° (polar angle measured from the flight direction) on one side and near 80° on the other, and that transition occurs at about 95°.

Shadowgraphs showed that the two spheres launched at a nominal Mach number of 1.5 (figs. 5(a) and (b)) had very different separation and transition patterns. On one sphere, transition occurred at or near separation; whereas, flow about the other sphere showed an asymmetric laminar separation over part of the body well ahead of transition. Shadowgraph prints of these two spheres at $M = 1.5$ are shown in figure 7. In figure 7(a) transition occurs at or very near separation, 105°. In figure 7(b) transition occurs near 105°, but separation occurs with a strong shock wave at 90° on one side and with weaker waves at 95° on the other. The sphere with the turbulent boundary layer at separation exhibited the more uniform motion (fig. 5(a)).

The surface-fixed shock waves prominent in figure 7(b), and seen in a more aft position in figure 7(a), occur at the junction between the ballast material and afterbody. Although it is conceivable that the interaction of the boundary layer and the surface shock waves could have contributed to the differences in flow separation and transition on the two spheres, this cannot be verified. Other differences in surface roughness could have also caused the observed differences in separation and transition.

Shadowgraphs from two tests in the subsonic regime showed a marked difference in the separation and transition. On one sphere the boundary layer was sometimes laminar and sometimes turbulent at separation. The separation was asymmetric and fluctuated with time. On the other sphere the boundary layer was always turbulent at separation which occurred at about 110°. Shadowgraph prints of these two spheres at $M = 0.56$ are presented in figure 8. In figure 8(a), laminar separation occurs ahead of the maximum diameter on one side (75°) and is delayed beyond the maximum diameter on the other side (95°). As mentioned previously, the direction of flight is nearly parallel to the horizontal reference wires. Transition occurs approximately 10° beyond the separation on both sides. The near wake is canted about 12° and gives the appearance of a widening wake on one side and a closing wake on the other. In figure 8(b), separation occurs near 110° on both sides, and the closure

angle of the near wake is approximately -5°. A comparison of the angular motions from these two tests is shown in figure 9, where it can be seen that the sphere with the turbulent boundary layer and delayed separation experienced a somewhat more regular motion.

The fluctuating asymmetrical separation of the boundary layer from the sphere introduces differences in the pressure distribution around the sphere which lead to a nonsteady normal force. This fluctuating normal force contributes to the erratic motions observed.

An attempt was made to determine these lateral forces by a correlation of the angular motions with the movements of the separation, transition, and wake closure angle. However, no direct correlation that was consistent throughout the tests could be found between the fluctuations in these parameters and the changes in model attitude. An example of this effort is shown in figure 10, where the flow parameters illustrated in the sketch are plotted against distance along the flight path. Included in figure 10 are the angles of attack and sideslip. As can be seen, the fluctuations in the flow parameters seem to bear some relation to the excursions in model attitude, but no quantitative correlation has been deduced from the information. The angular motion, as viewed in the α-β plane, is shown in figure 3(e).

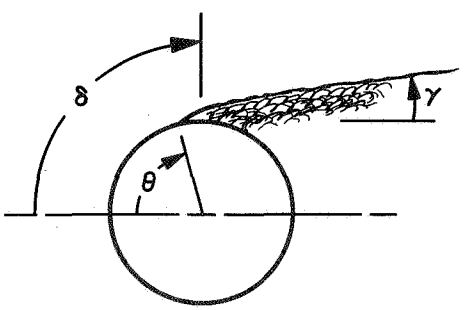

Variations of these flow parameters with Mach number and/or Reynolds number became evident and are shown in figure 11, where the average values are plotted as functions of Mach number. Figure 11 shows the laminar separation angle, θ, and the wake angle, γ, in the supersonic and hypersonic regimes. As the Mach number is increased in the low supersonic regime, separation rapidly moves back beyond the maximum diameter accompanied by a convergence of the wake. Negative values of γ indicate a converging wake. At Mach numbers from 5 to 15 the separation is at about 116° polar angle measured from the direction of flight. The wake angle is steepest at -16° near a Mach number of 5 when transition occurs about one-half body diameter behind the sphere, as seen in figure 12(a). In the hypersonic regime, the wake closure angle is about -12° and transition is almost one body diameter behind the sphere (fig. 12(b)). (The apparent distortion of the front of the spheres in figure 12 is an optical effect due to refraction of the light by the shock wave.)

Figure 13 shows the boundary-layer-flow parameters in the subsonic and low supersonic regimes. Values of θ and γ from the shadowgraphs which showed a laminar boundary layer at separation are plotted in figure 13(a) along with values of the polar angle at which transition occurs, δ. The open symbols indicate when separation was laminar throughout the flight. The partially filled symbols indicate the laminar-separation observations from flights that were intermittently turbulent. The number of measurements available at each Mach number was from 10 to 150. The bars indicate the standard

deviation from the arithmetic mean of the data and, statistically, best represent the uncertainty in the values due to both random errors and real differences in the measurements. These data are plotted against Mach number but would show the same characteristics if plotted against Reynolds number. In the present tests the Reynolds number varies linearly with Mach number in this speed range so their effects on the data cannot be separated.

As the Mach number is decreased to 0.9, the separation and transition move forward accompanied by a widening of the wake. Transition occurs about 15° beyond separation, and the inclination of the edge of the wake is approximately the same as a tangent to the sphere at separation. The spheres which experienced some turbulent separation during the flight showed a delayed laminar separation and early transition compared with the totally laminar flights, but the wake angle was not affected. As the Mach number is further decreased, separation and transition move back again and the wake becomes narrower. Transition occurs about 10° beyond separation, and the inclination of the edge of the wake is approximately 5° less than a tangent to the sphere at separation.

The values of θ and γ from the shadowgraphs which showed a turbulent boundary layer at separation are plotted in figure 13(b). The closed symbols indicate turbulent separation throughout the flight. The partially filled symbols indicate the turbulent-separation observations from flights that were intermittently laminar. As the Mach number is decreased to 0.9, the separation moves forward and is accompanied by a widening of the wake, similar to the laminar flow. However, the similarity does not hold below a Mach number of 0.7. The turbulent separation moves sharply back beyond the maximum diameter at a Mach number of 0.55, and the wake strongly converges. As the Mach number is decreased to 0.4, separation moves forward again toward the maximum diameter, and the wake becomes divergent.

The values of θ and γ from figures 13(a) and (b) (plotted together in fig. 13(c)) show that in the Mach number range from 0.7 to 1.7, turbulence delays separation about 10° but has little or no effect on the wake angle. At the two low Mach numbers, the large standard deviations are shown by the bars. The wake angle is not well defined, and the wake could be converging or diverging. Turbulence delays separation well beyond the maximum diameter at $M = 0.55$ but has less effect on the location of separation at $M = 0.4$.

Drag

The variation of drag coefficient, C_D, with Mach number is shown in figure 14. In this and subsequent figures the open symbols indicate tests in which the boundary layer was always laminar at separation, the closed symbols indicate turbulent flow at separation, and the partially filled symbols indicate tests in which the state of the boundary layer at separation varied during the flight.

Figure 14(a) shows that C_D is constant at 0.89 in the hypersonic regime, increases to a maximum of 0.98 in the low supersonic regime, and decreases rapidly through the subsonic regime. The flagged symbol at a

nominal Mach number of 9 indicates a test conducted at a higher Reynolds number (1.0×10^6) than the other tests at this speed (0.5×10^6). The increased Reynolds number was obtained by increasing the test-section air pressure from one-fourth to one-half atmospheric pressure. The measured drag coefficient at this increased Reynolds number is slightly higher at 0.90, and agrees with sphere drag data at $R = 1.1\times10^6$ reported in reference 12. The higher drag coefficient (0.92) reported in reference 4 was measured at a Reynolds number near 2×10^6 and indicates there may be a slight increase in C_D with Reynolds number in the hypersonic regime.

Figure 14(b) shows the variation of C_D with Mach number in the subsonic regime. The Reynolds number varies from 0.4×10^6 to 1.0×10^6 linearly with Mach number. As is well known with spheres at subsonic speeds, when the Mach number and Reynolds number are decreased, the drag coefficient becomes increasingly dependent on the boundary-layer-flow conditions near separation.

Static Stability

Static-stability data are presented in figure 15, where the pitching-moment-curve slope, C_{m_α}, is plotted as a function of Mach number. The data points were obtained from the wavelength of pitching oscillation, as mentioned previously. The static stability is nearly constant in the hypersonic regime and decreases in the subsonic regime. The scatter in the data increases as the Mach number is decreased through the low supersonic and into the subsonic regimes. It appears that the static stability depends on the boundary-layer-flow conditions near separation. At the same flight conditions, the static stability is greater for the spheres which experienced some turbulence at separation.

The curve in the figure represents the product of the drag coefficient and the static margin. In the absence of lateral forces, the pitching moment is equal to the component of drag normal to the longitudinal axis, $C_D \sin\alpha$, times the static margin, $\bar{x}$. In the hypersonic regime, most of the data are within 7 percent of the values shown by the curve. This agreement is consistent with the symmetry in the flow-separation patterns and angular motions observed at these speeds.

Dynamic Stability

Dynamic-stability data are presented in figure 16, where the dynamic-stability parameter, ξ, is plotted as a function of Mach number. The parameter, ξ, is related to the aerodynamic coefficients by

$$\xi = C_D - C_{L_\alpha} + (C_{m_q} + C_{m_{\dot{\alpha}}})(d/\sigma)^2$$

The bars indicate the uncertainty in the values of ξ due to random experimental errors, as calculated by the method described in reference 13. In

most cases the standard deviation in ξ is less than 1. Positive values of ξ indicate a growth in amplitude of oscillation, thus dynamic instability.

As can be seen in the figure, there is no clear trend or predictable variation of ξ with Mach number. At the same test conditions ξ differs by more than the uncertainty in the data. The data show the ballasted sphere to be dynamically unstable, except for the two negative values of ξ, at $M = 0.8$ and 13.5. No explanation can be given for these two values. The angular motions did show a decay in amplitude of oscillation; however, the type of motion (i.e., nearly planar oscillation), the amplitude of oscillation, and the boundary-layer-flow separation of these two flights were similar to those of the other flights at comparable Mach numbers.

In the subsonic regime, most of the angular motions showed an erratic growth in amplitude, definitely indicative of dynamic instability, but which could not be reduced to a coefficient form.

CONCLUDING REMARKS

Experimental measurements have been made of the dynamic-flight behavior of a ballasted sphere, with a static margin of 14 percent of the diameter, over a Mach number range from 0.4 to 14.5 and Reynolds number range from 0.4×10^6 to 1.6×10^6. From examinations of the flow fields and analyses of the motions, stability, and drag data the following conclusions can be drawn.

The ballasted sphere is dynamically unstable over the entire range of test conditions.

At supersonic and hypersonic speeds, laminar separation occurs well beyond the maximum diameter, and the wake strongly converges. The flow-separation patterns are symmetrical about the sphere, which exhibits no erratic flight motions. The angular motions are nearly planar oscillations which grow in amplitude, thereby demonstrating dynamic instability. The static stability and drag coefficient are nearly constant. The measured static stability, symmetry in flow-separation patterns, and nearly planar oscillations all point to the absence of lateral forces on the sphere at high speeds.

In the low supersonic regime, separation moves forward with decreasing Mach number and Reynolds number and reaches the maximum diameter of the sphere near a Mach number of 1.4, where the edge of the wake becomes parallel to the flight direction. Turbulence delays separation and causes the sphere to be more stable statically but has little or no effect on the wake angle or the drag coefficient.

At subsonic speeds, separation reaches the most forward position on the sphere and is accompanied by a strongly divergent wake at a Mach number near 0.8. Below a Mach number of 0.6, the wake may converge, diverge, or be parallel to the flight direction as the separation moves back toward the maximum

diameter. The angular motions are very erratic. Fluctuations in the separation and wake angles increase in magnitude as the Mach number and Reynolds number decrease. Turbulence delays separation well beyond the maximum diameter at $M = 0.55$ ($R = 0.52 \times 10^6$) and causes a large reduction in the drag coefficient.

The ballasted sphere would appear to be suitable as an atmosphere probe during high-speed entry if a damping system could alleviate the dynamic instability. Its applicability as a probe at subsonic speeds probably depends on controlling flow-separation patterns around the sphere which might sacrifice the major advantage of the spherical shape, namely, a drag coefficient independent of angle of attack.

Ames Research Center
National Aeronautics and Space Administration
Moffett Field, Calif., 94035, July 13, 1967
129-01-08-02-00-21

REFERENCES

1. Seiff, Alvin: Some Possibilities for Determining the Characteristics of the Atmospheres of Mars and Venus From Gas-Dynamic Behavior of a Probe Vehicle. NASA TN D-1770, 1963.

2. Peterson, Victor L.: A Technique for Determining Planetary Atmosphere Structures From Measured Accelerations of an Entry Vehicle. NASA TN D-2669, 1965.

3. Seiff, Alvin; and Reese, David E., Jr.: Use of Entry Vehicle Responses to Define the Properties of the Mars Atmosphere. AAS Preprint 65-24, 1965.

4. Hodges, A. J.: The Drag Coefficient of Very High Velocity Spheres. J. Aeron. Sci., vol. 24, no. 10, Oct. 1957.

5. Lehnert, R.: Base Pressure of Spheres at Supersonic Speeds. NAVORD Rep. 2774, 1953.

6. Sabin, C. M.: The Effects of Reynolds Number, Mach Number, Spin Rate, and Other Variables on the Aerodynamics of Spheres at Subsonic and Transonic Velocities. BRL Memo Rep. 1044, 1956.

7. Charters, A. C.; and Thomas, R. N.: The Aerodynamic Performance of Small Spheres from Subsonic to High Supersonic Velocities. J. Aeron. Sci., vol. 12, no. 4, 1945.

8. Sommer, Simon C.; Boissevain, Alfred G.; Yee, Layton; and Hedlund, Roger C.: The Structure of an Atmosphere From On-Board Measurements of Pressure, Temperature, and Acceleration. NASA TN D-3933, 1967.

9. Seiff, Alvin: A Free-Flight Wind Tunnel for Aerodynamic Testing at Hypersonic Speeds. NACA Rep. 1222, 1955.

10. Seiff, Alvin: A New Method for Computing Drag Coefficients From Ballistic Range Data. J. Aeron. Sci., vol. 25, no. 2, Feb. 1958.

11. Short, Barbara J.; and Sommer, Simon C.: Some Measurements of the Dynamic and Static Stability of Two Blunt-Nosed, Low-Fineness-Ratio Bodies of Revolution in Free Flight at M = 4. NASA TM X-20, 1959.

12. Seiff, Alvin; Sommer, Simon C.; and Canning, Thomas N.: Some Experiments at High Supersonic Speeds on the Aerodynamic and Boundary-Layer Transition Characteristics of High-Drag Bodies of Revolution. NACA RM A56I05, 1957.

13. Chapman, Gary T.; and Kirk, Donn B.: Problems Associated With Obtaining Accurate Dynamic Stability Results From Free-Flight Tests. Presented at 2nd Technical Workshop on Dynamic Stability Testing, AEDC, April 1965.

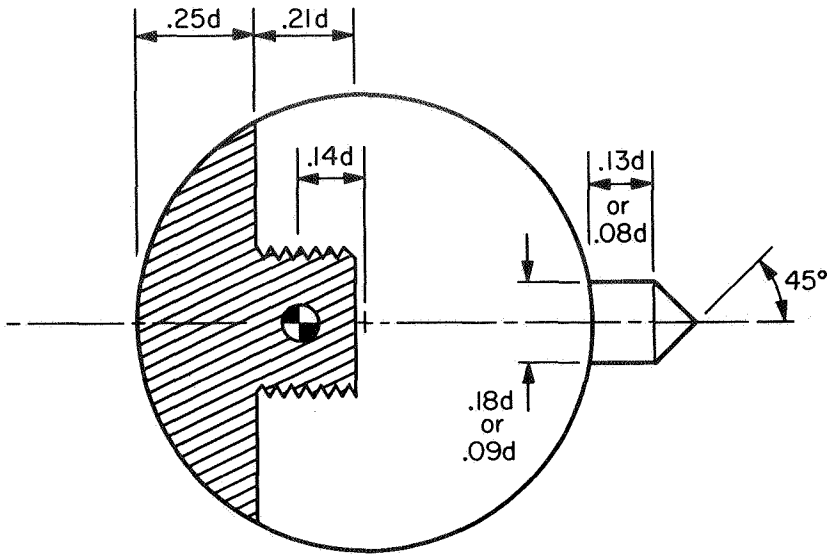

(a) Aluminum sphere ballasted with a tungsten alloy; I_y/I_x = 1.2, d = 0.4 or 1.6 inches.

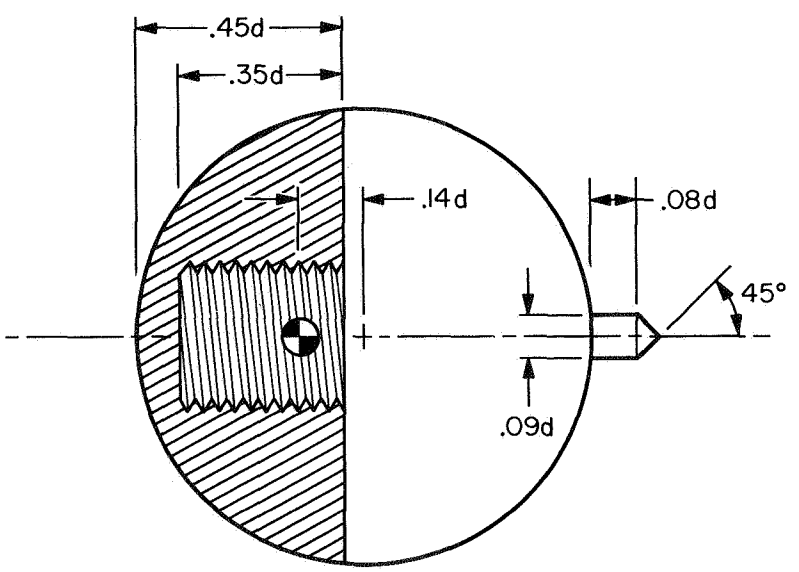

(b) Nylon sphere ballasted with steel; I_y/I_x = 0.8, d = 1.6 inches.

Figure 1.- Sketch of models.

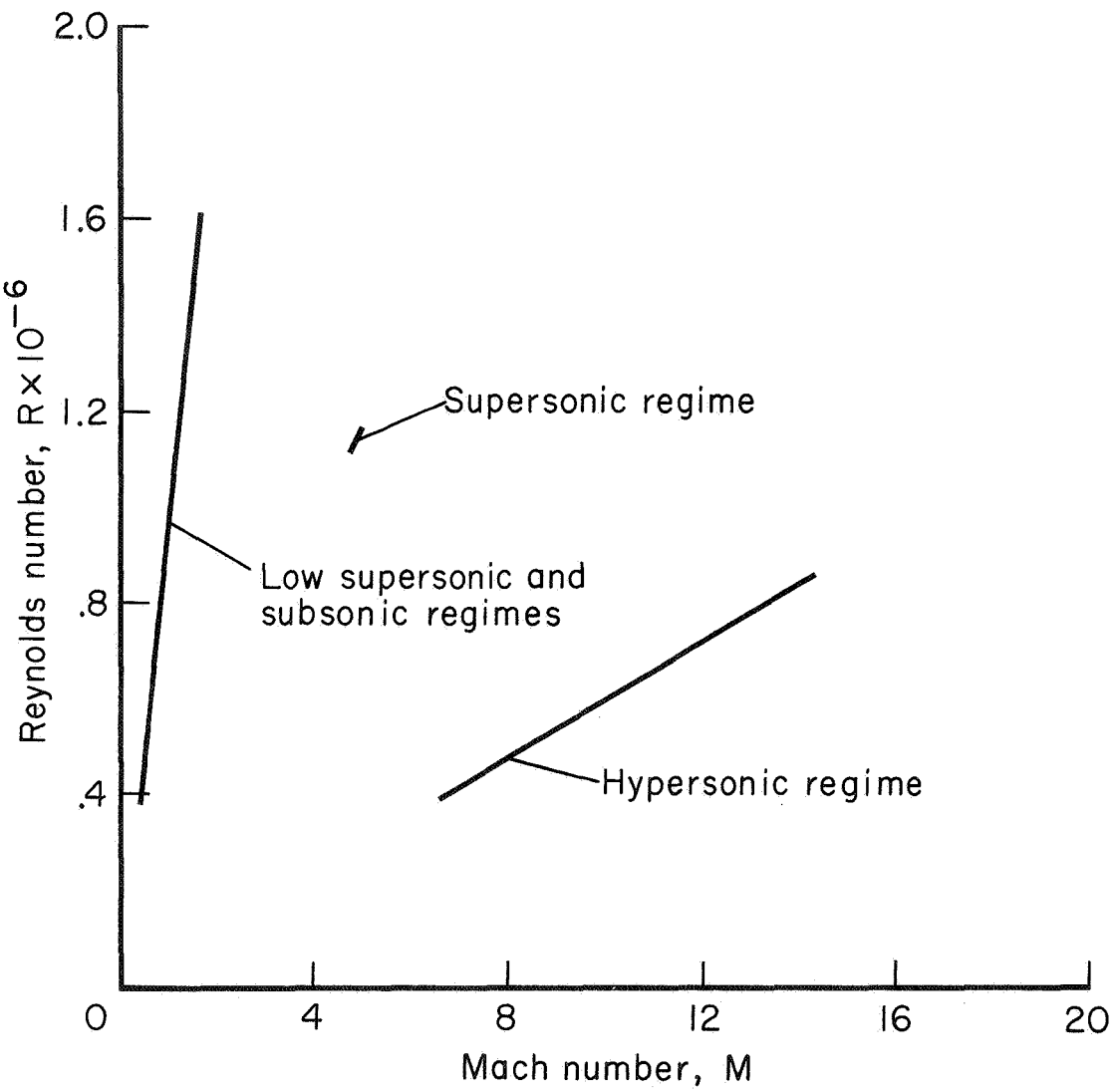

Figure 2.- Nominal test conditions.

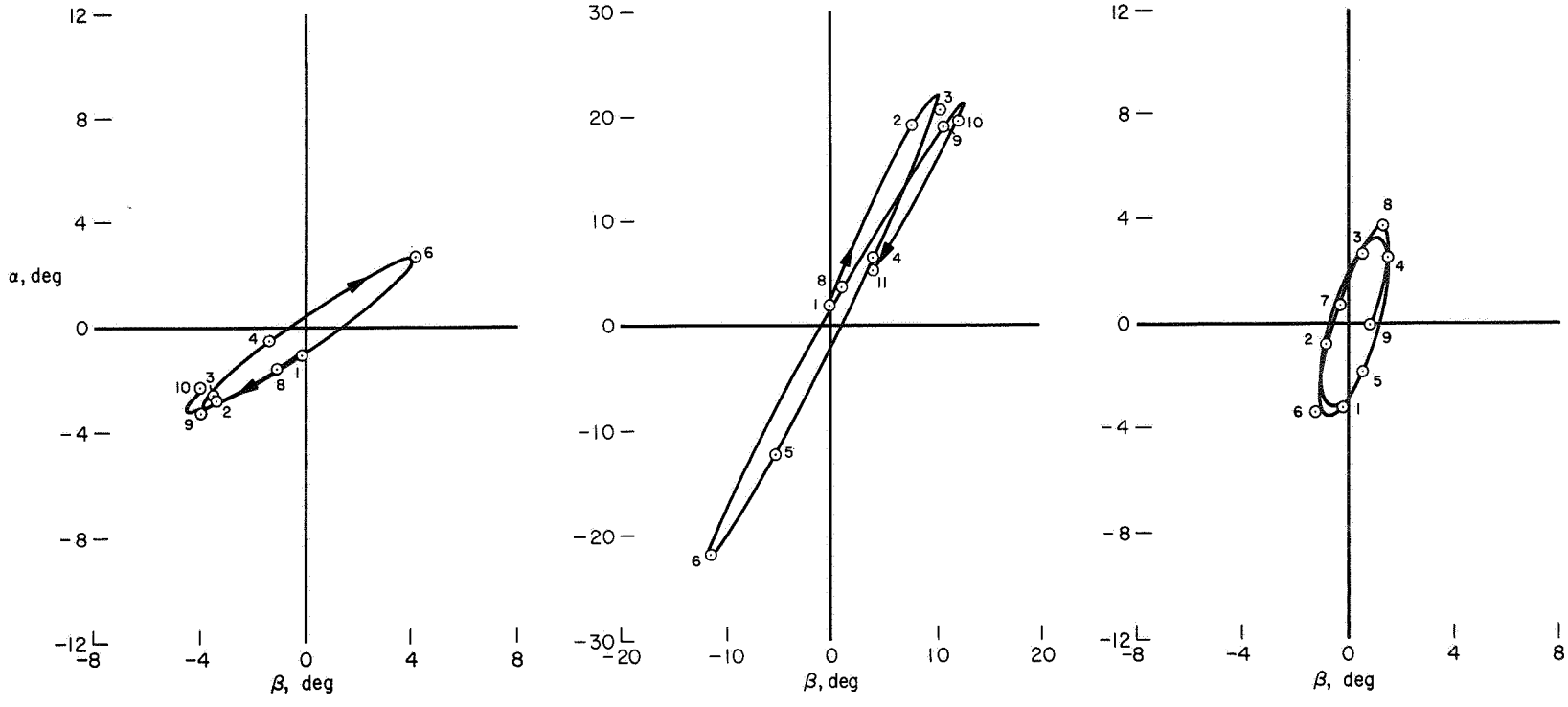

(a) M = 13.0, R = 0.8×10^6 (b) M = 9.2. R = 0.6×10^6 (c) M = 4.8, R = 1.1×10^6

Figure 3.- Angular motions of a ballasted sphere; $I_y/I_x = 1.2$.

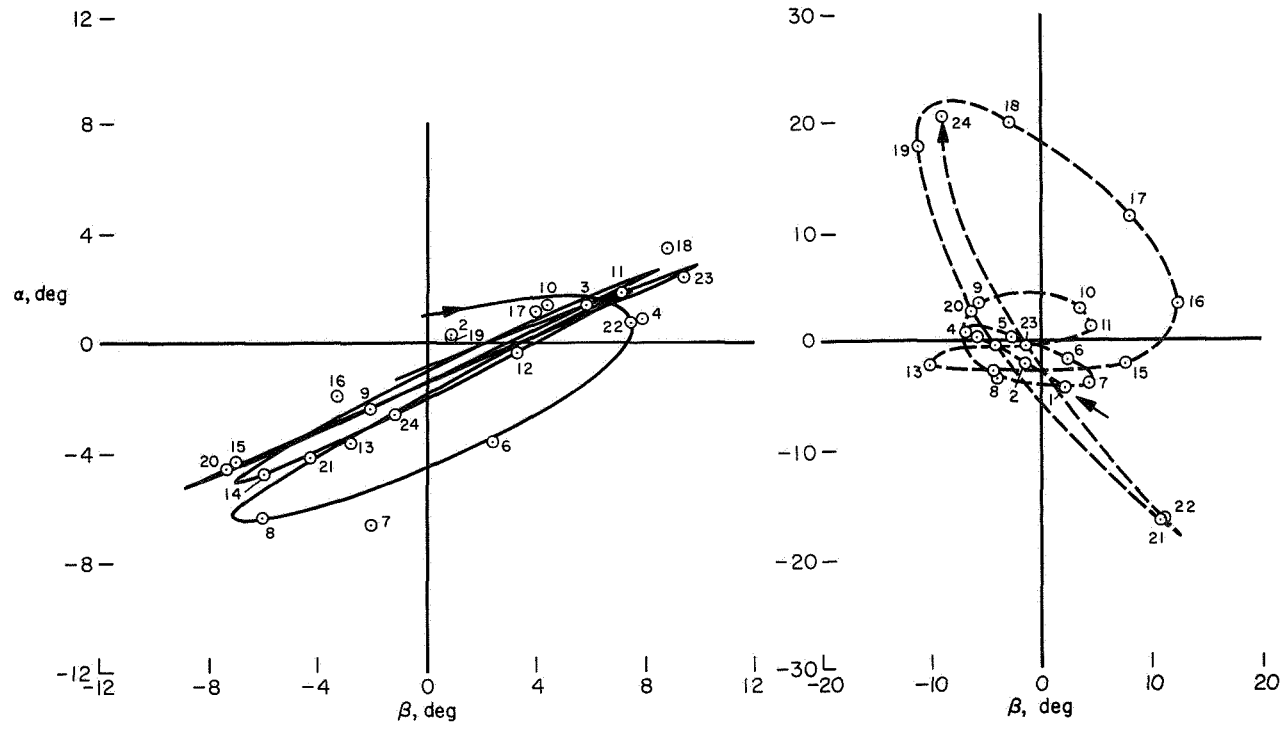

(d) M = 0.9, R = 0.8x10^6

(e) M = 0.8, R = 0.8x10^6

Figure 3.- Concluded.

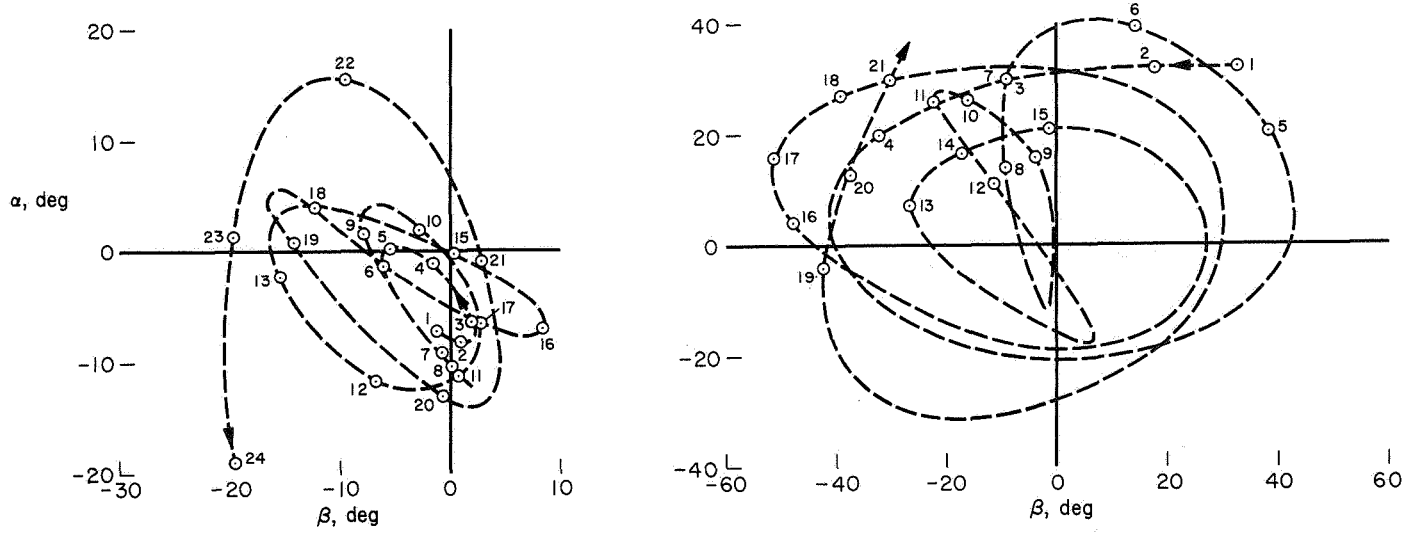

(a) 1.6-inch-diameter ballasted sphere in ballistic range at M = 0.7, R = 0.7×10^6; I_y/I_x = 1.2.

(b) 2-foot-diameter ballasted sphere in free fall at M = 0.5, R = 2.0×10^6; I_y/I_x = 0.9.

Figure 4.- Comparison of angular motions obtained in free fall and in the ballistic range.

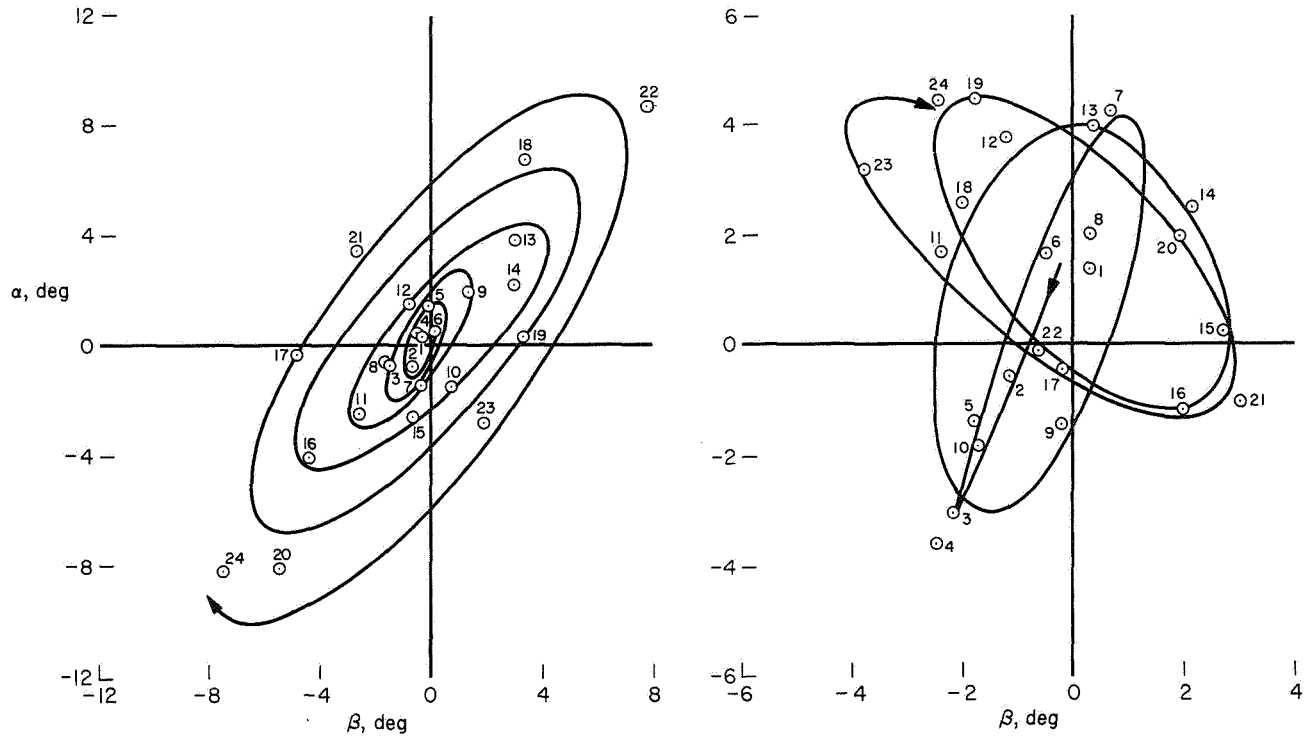

(a) $I_y/I_x = 0.8$; M = 1.5, R = 1.5×10^6 (b) $I_y/I_x = 1.2$; M = 1.5, R = 1.5×10^6

Figure 5.- Comparison of angular motions of sphere with different inertia ratios.

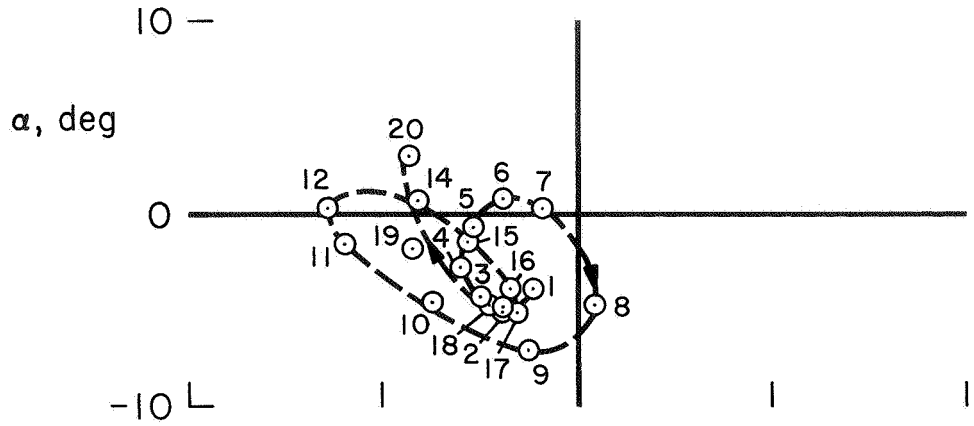

(c) I_y/I_x = 1.2; M = 1.0, R = 0.9×10^6

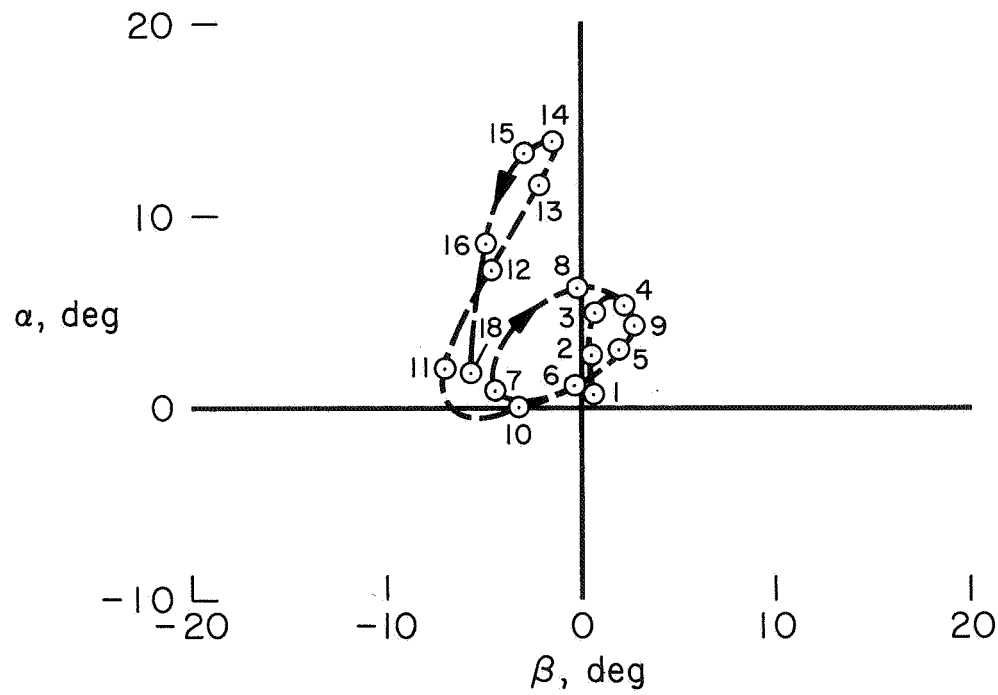

(d) I_y/I_x = 0.8; M = 1.0, R = 0.9×10^6

Figure 5.- Concluded.

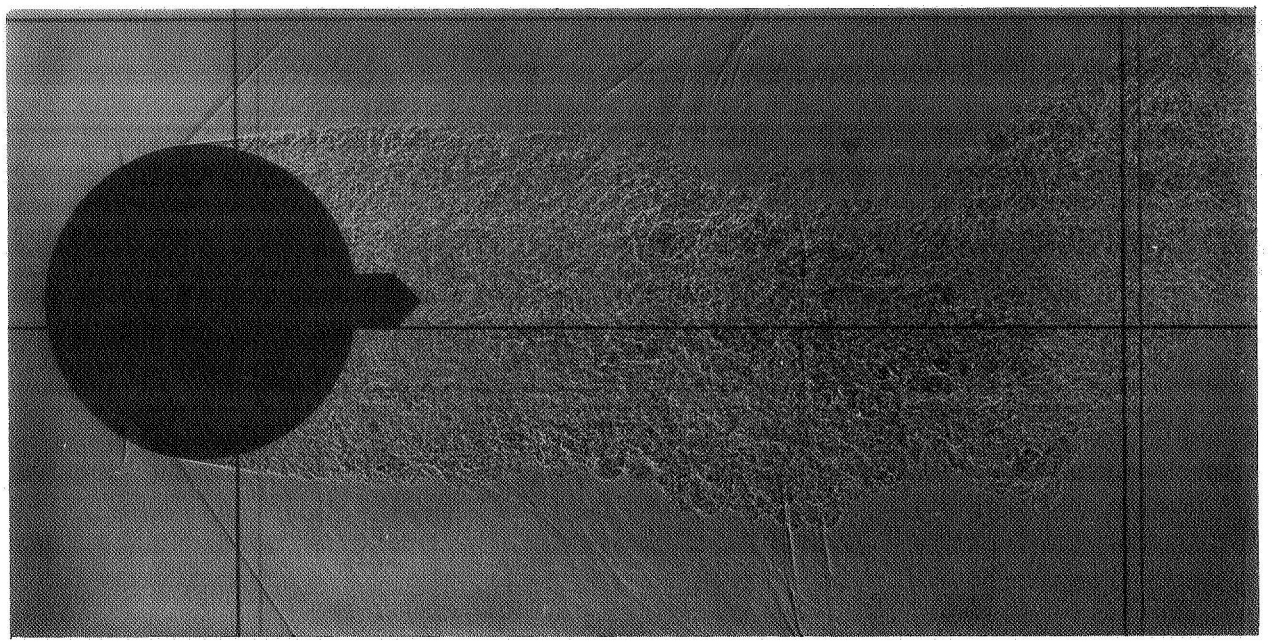

(a) Laminar separation; $\alpha = 0.8^{\circ}$ ($\beta = 5.4^{\circ}$); $I_y/I_x = 1.2$ (see fig. 5(c)).

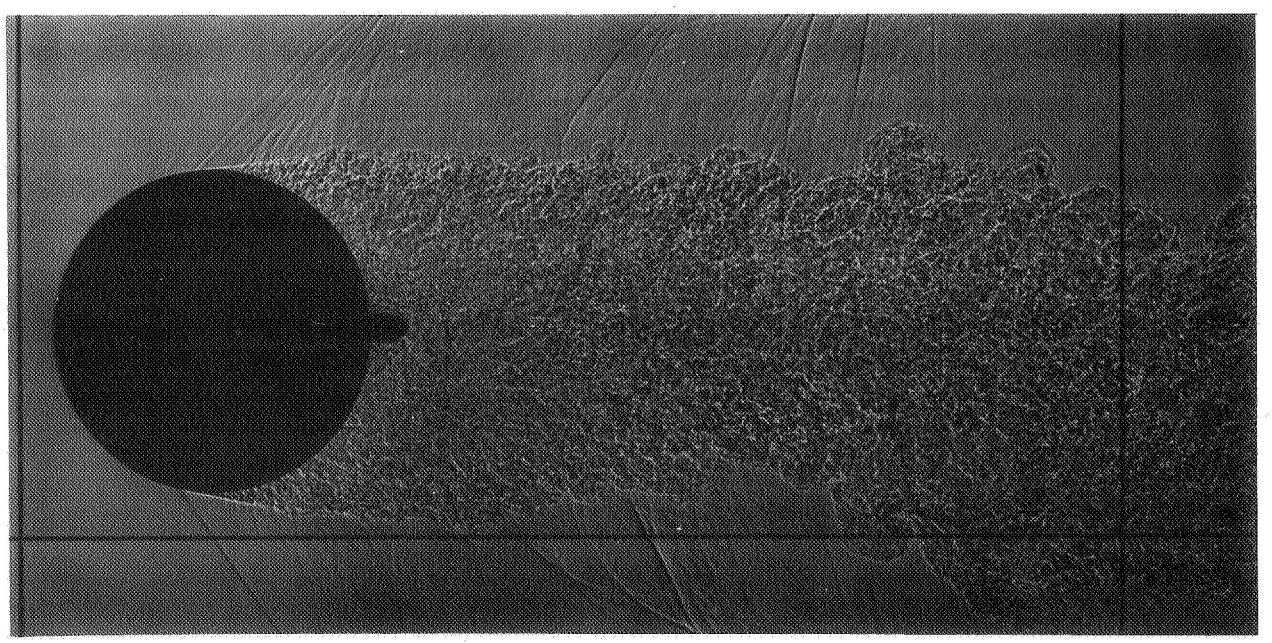

(b) Laminar separation; $\alpha = 1.2^{\circ}$ ($\beta = 0.3^{\circ}$); $I_y/I_x = 0.8$ (see fig. 5(d)).

Figure 6.- Shadowgraphs of ballasted sphere at M = 1.0, R = 1.0×10^6.

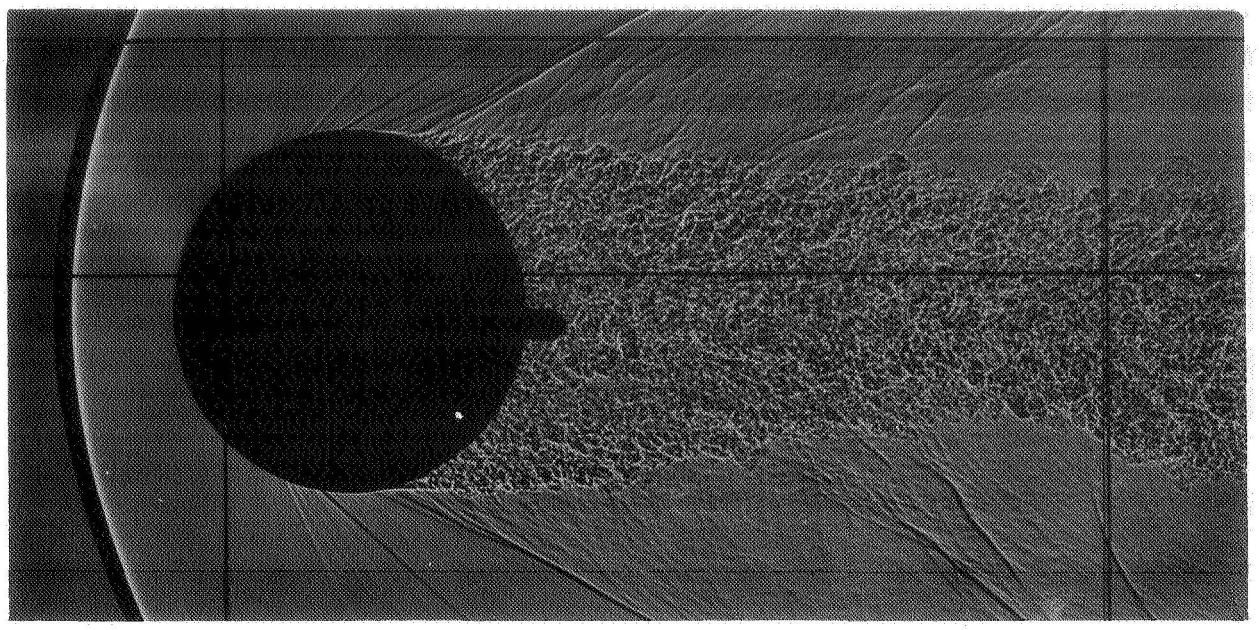

(a) Transition near separation; $\alpha = 3.8^{\circ}$ ($\beta = 3.0^{\circ}$); $I_y/I_x = 0.8$ (see fig. 5(a)).

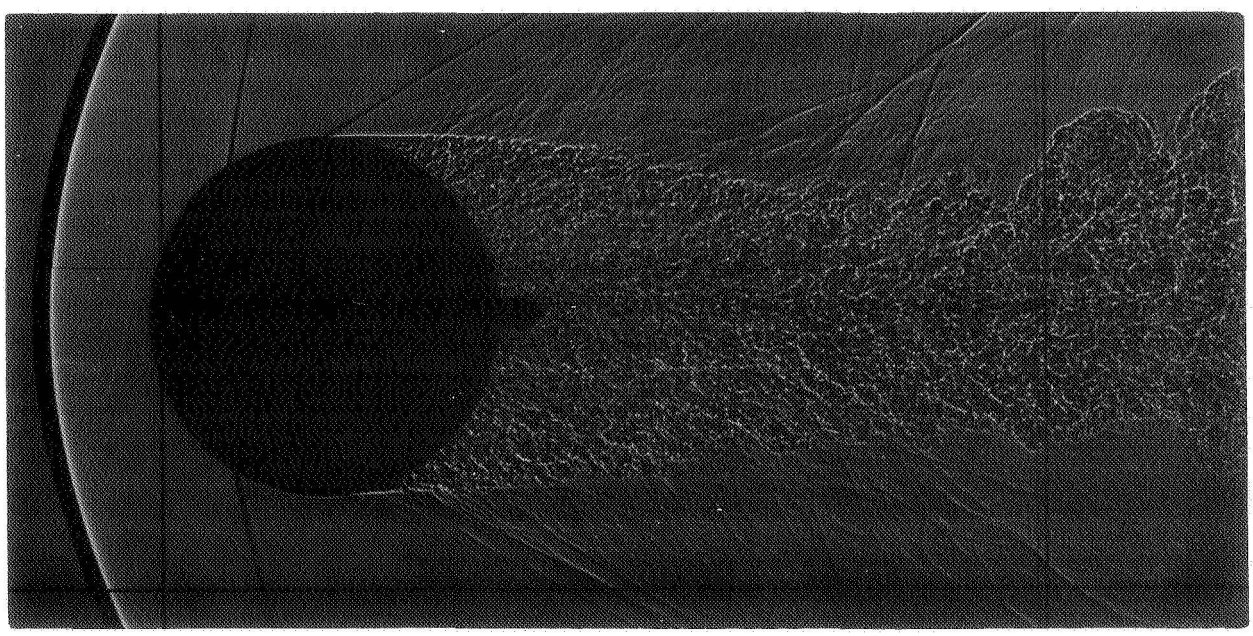

(b) Asymmetric separation; $\alpha = 0.5^{\circ}$ ($\beta = 0.2^{\circ}$); $I_y/I_x = 1.2$ (see fig. 5(b)).

Figure 7.- Shadowgraphs of ballasted sphere at M = 1.5, R = 1.4×10^6.

(a) Asymmetric laminar separation; $\alpha = 6.8^{\circ}$ ($\beta = 4.8^{\circ}$); $I_y/I_x = 1.2$.

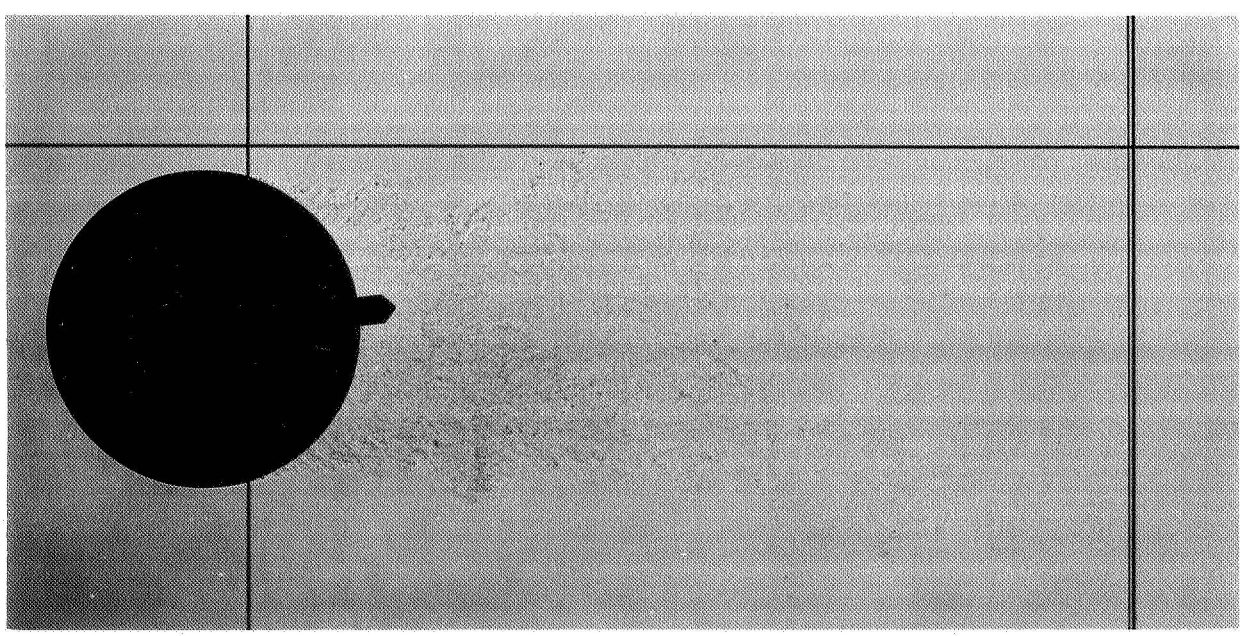

(b) Turbulent separation; $\alpha = 5.6^{\circ}$ ($\beta = 2.0^{\circ}$); $I_y/I_x = 0.8$.

Figure 8.- Shadowgraphs of ballasted sphere at M = 0.56, R = 0.53×10^6.

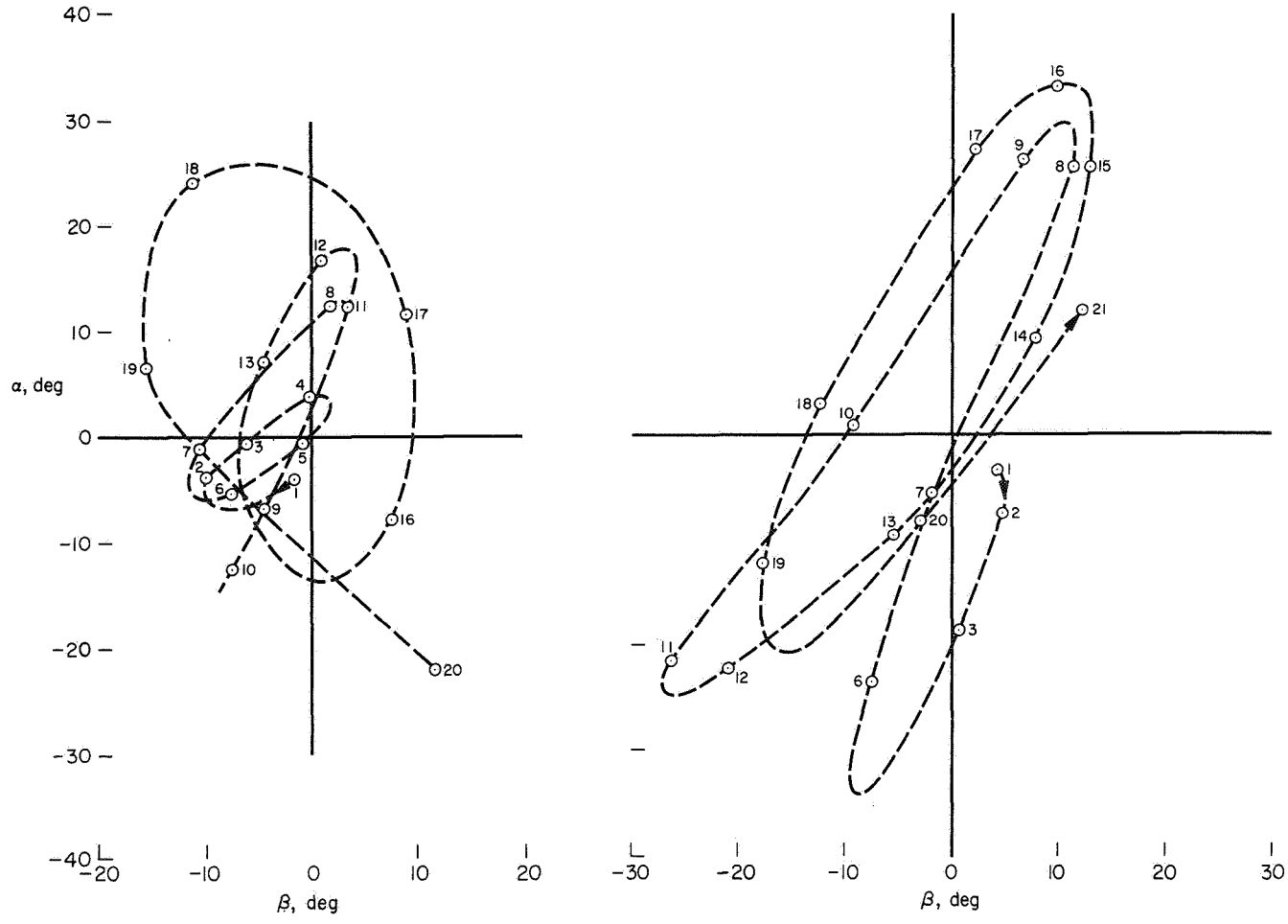

(a) Motion of sphere with asymmetric laminar flow separation as seen in figure 8(a); $I_y/I_x = 1.2$.

(b) Motion of sphere with turbulent flow separation as seen in figure 8(b); $I_y/I_x = 0.8$.

Figure 9.- Angular motions of ballasted sphere at M = 0.55, R = 0.52×10^6.

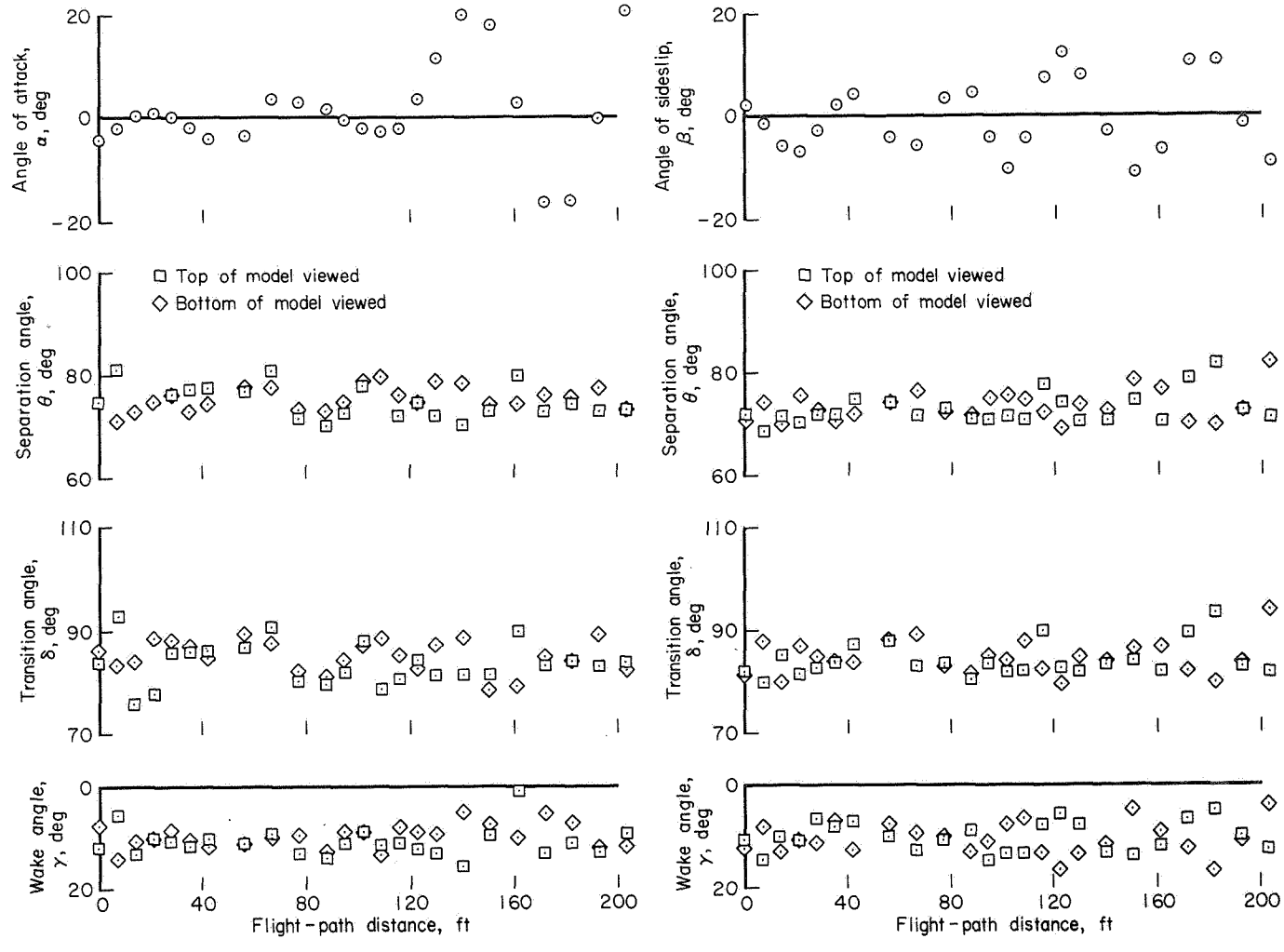

(a) Vertical plane.

(b) Horizontal plane.

Figure 10.- Angular motion and flow parameters along the flight trajectory (see fig. 3(e)); M = 0.8.

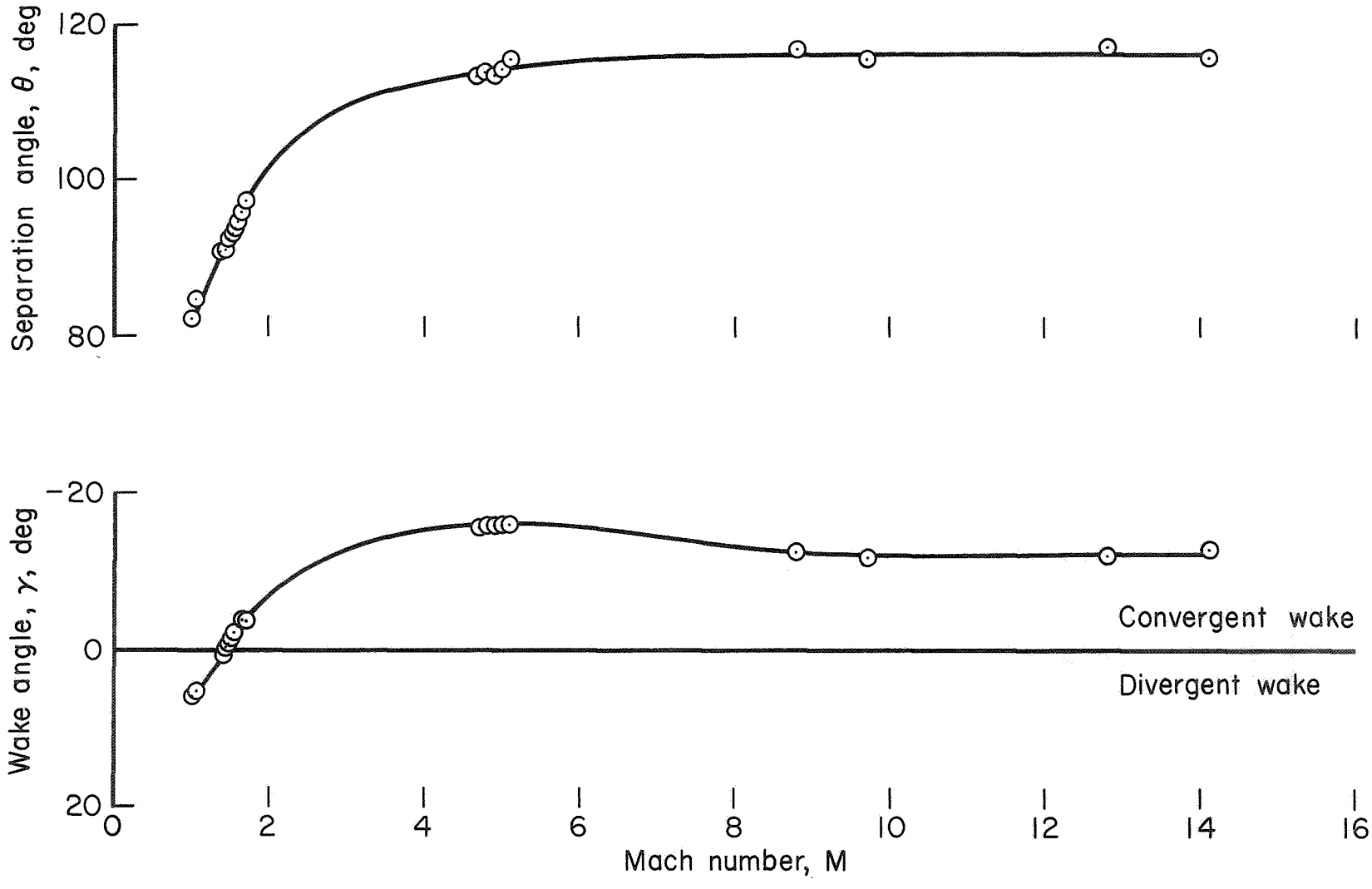

Figure 11.- Separation and wake-angle parameters in the supersonic and hypersonic regimes; laminar flow at separation.

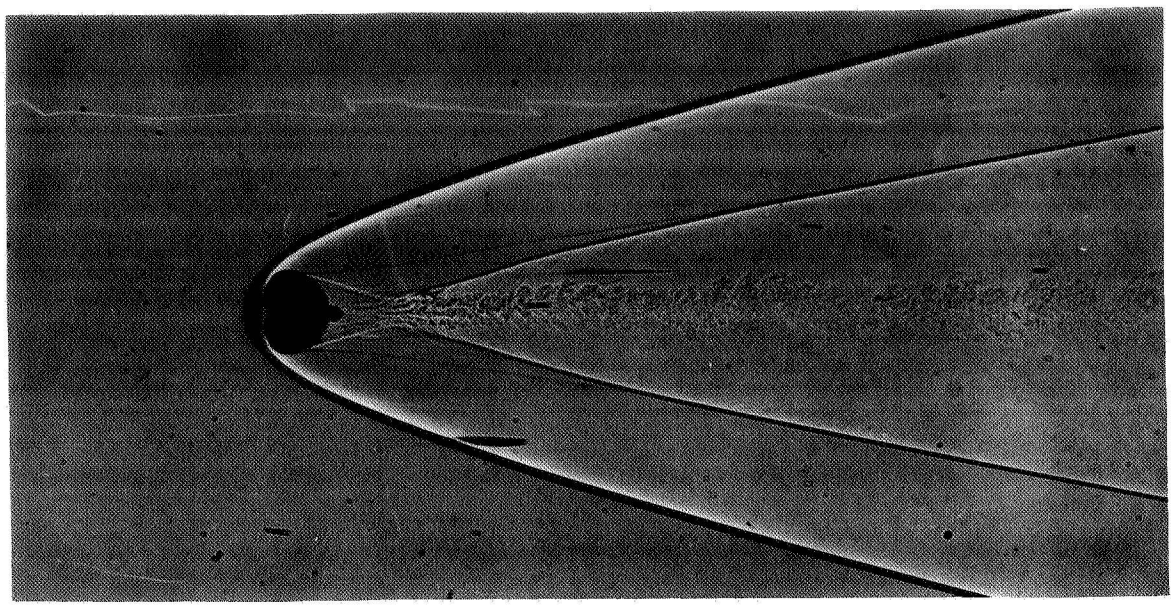

(a) M = 5.1, R = 1.2×10^6; $\alpha = 2^\circ$ ($\beta = 1^\circ$)

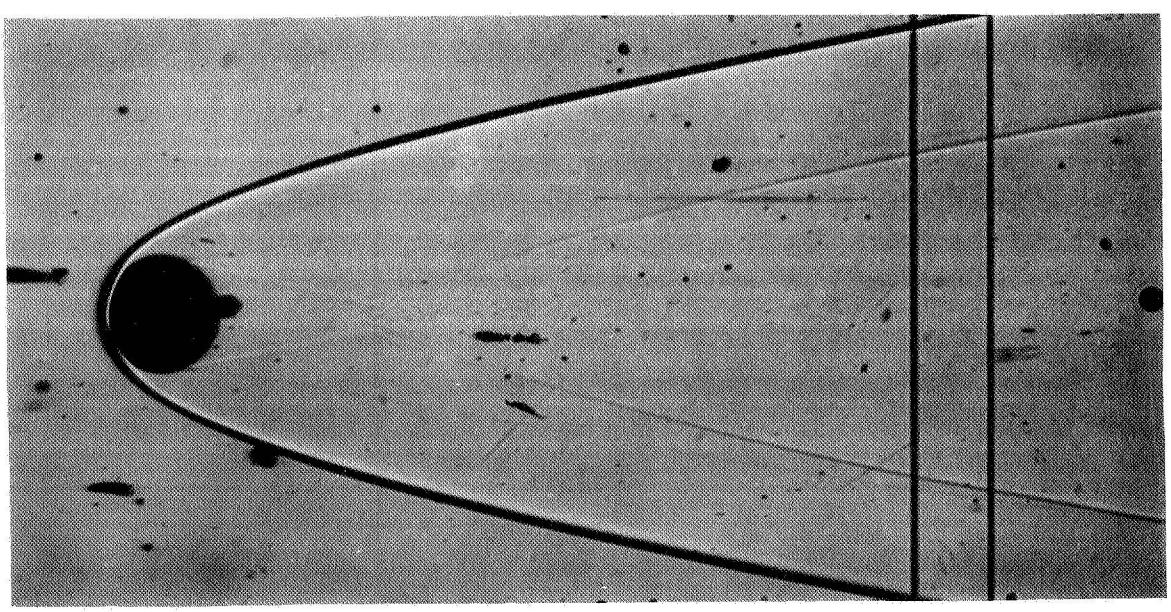

(b) M = 9.2, R = 0.6×10^6; $\alpha = 6^\circ$ ($\beta = 4^\circ$)

Figure 12.- Shadowgraphs of ballasted sphere at high speeds.

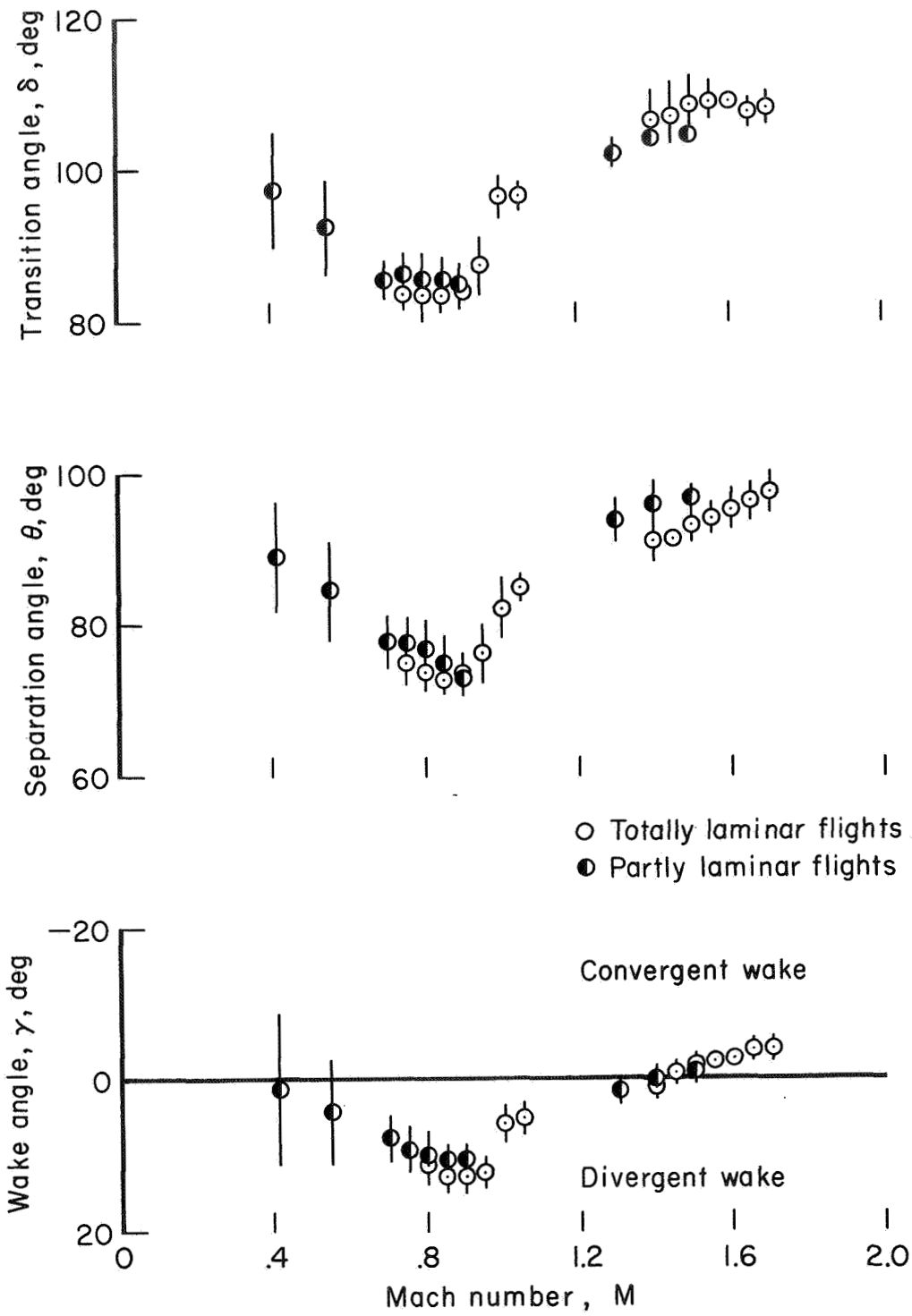

(a) Laminar flow at separation.

Figure 13.- Transition, separation, and wake-angle parameters in the subsonic and low supersonic regimes.

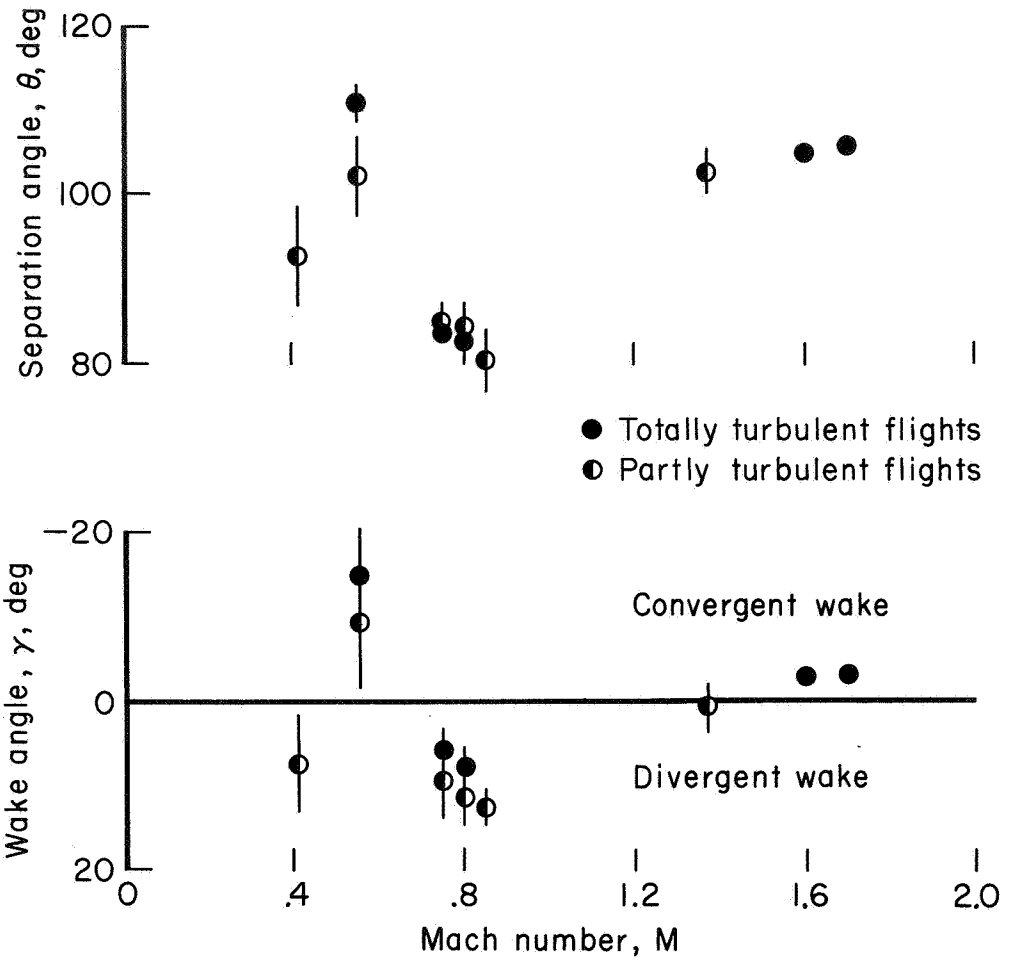

(b) Turbulent flow at separation.

Figure 13.- Continued.

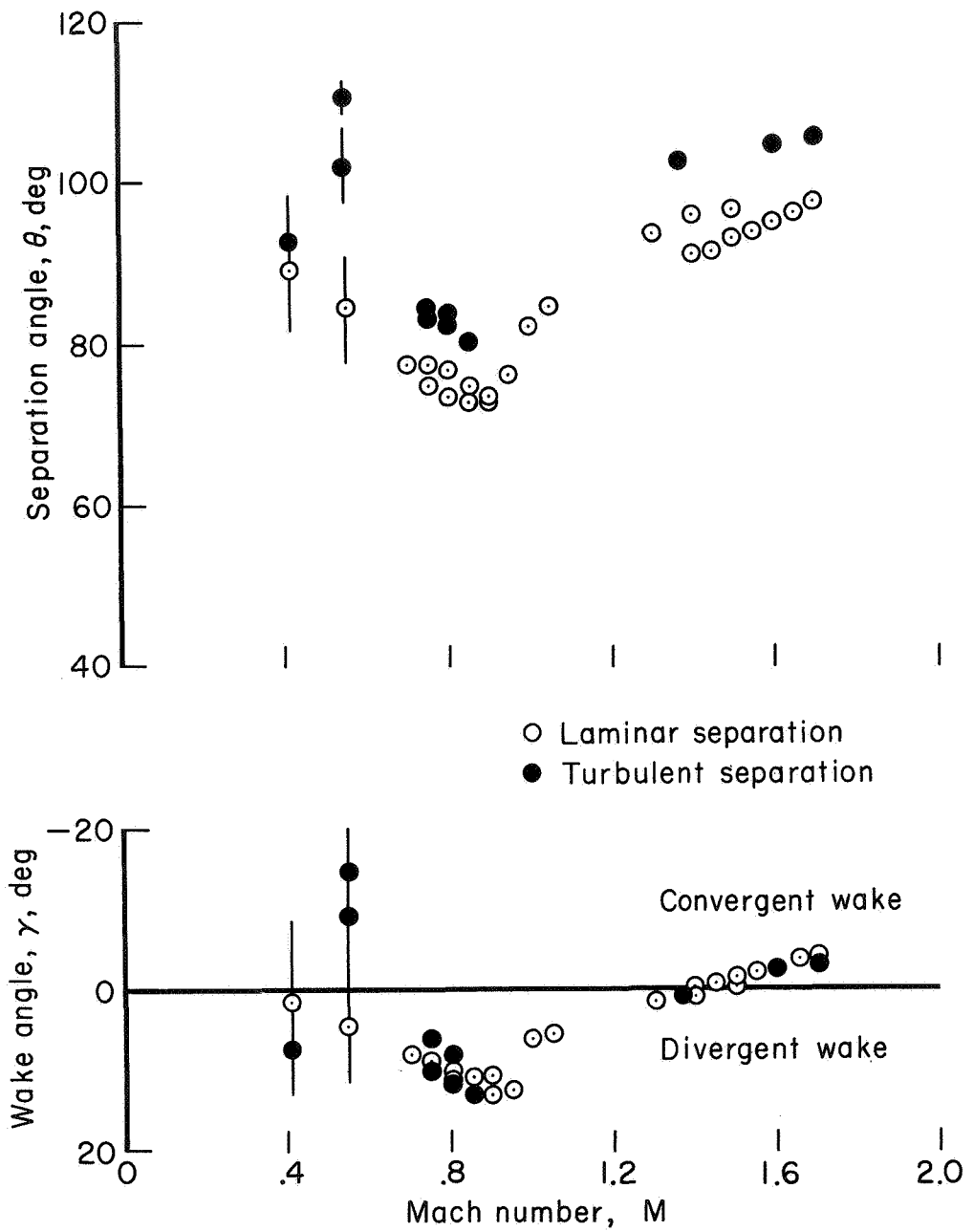

(c) Effect of turbulence on separation and wake angles.

Figure 13.- Concluded.

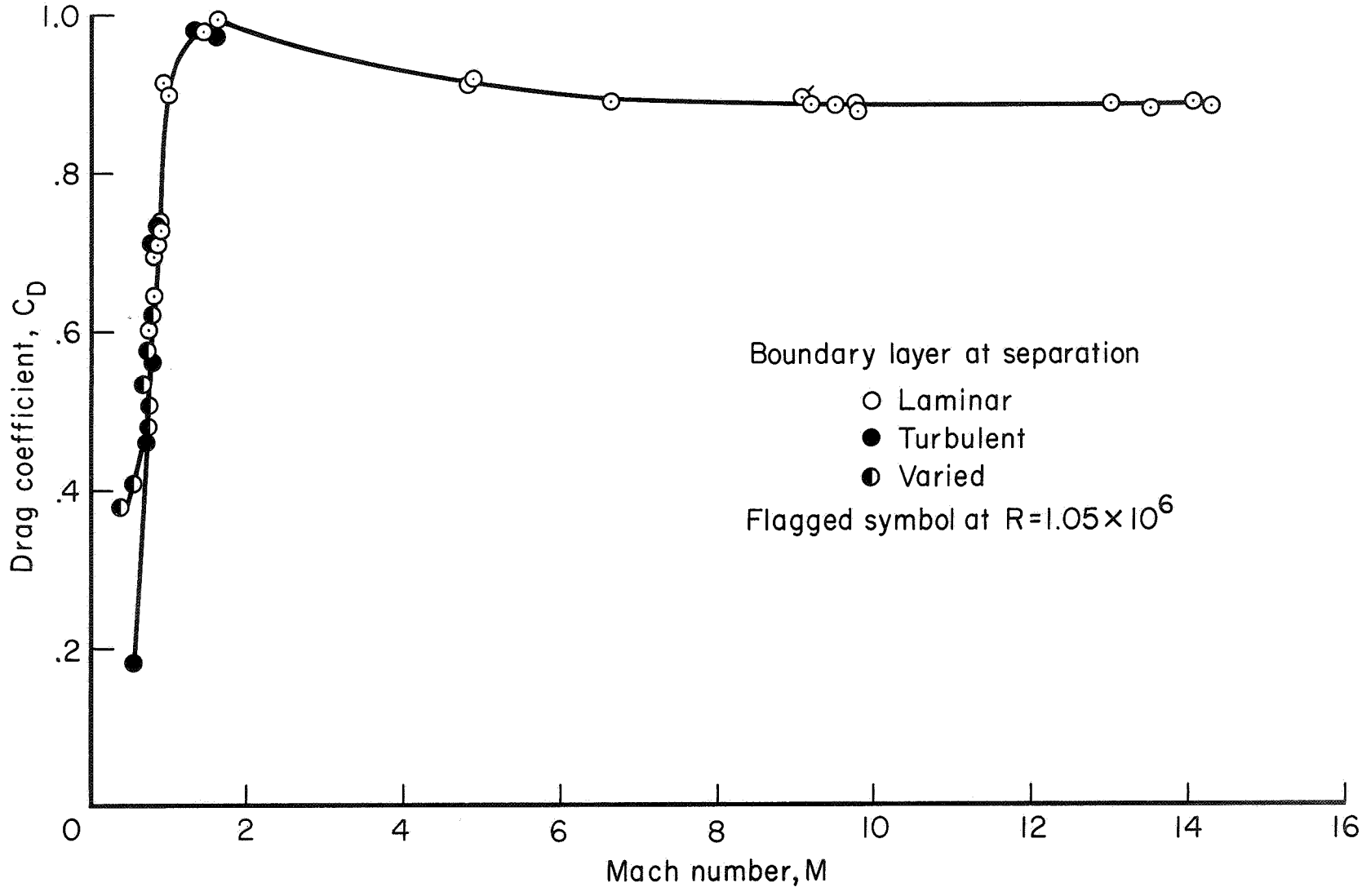

(a) All speed regimes.

Figure 14.- Drag data.

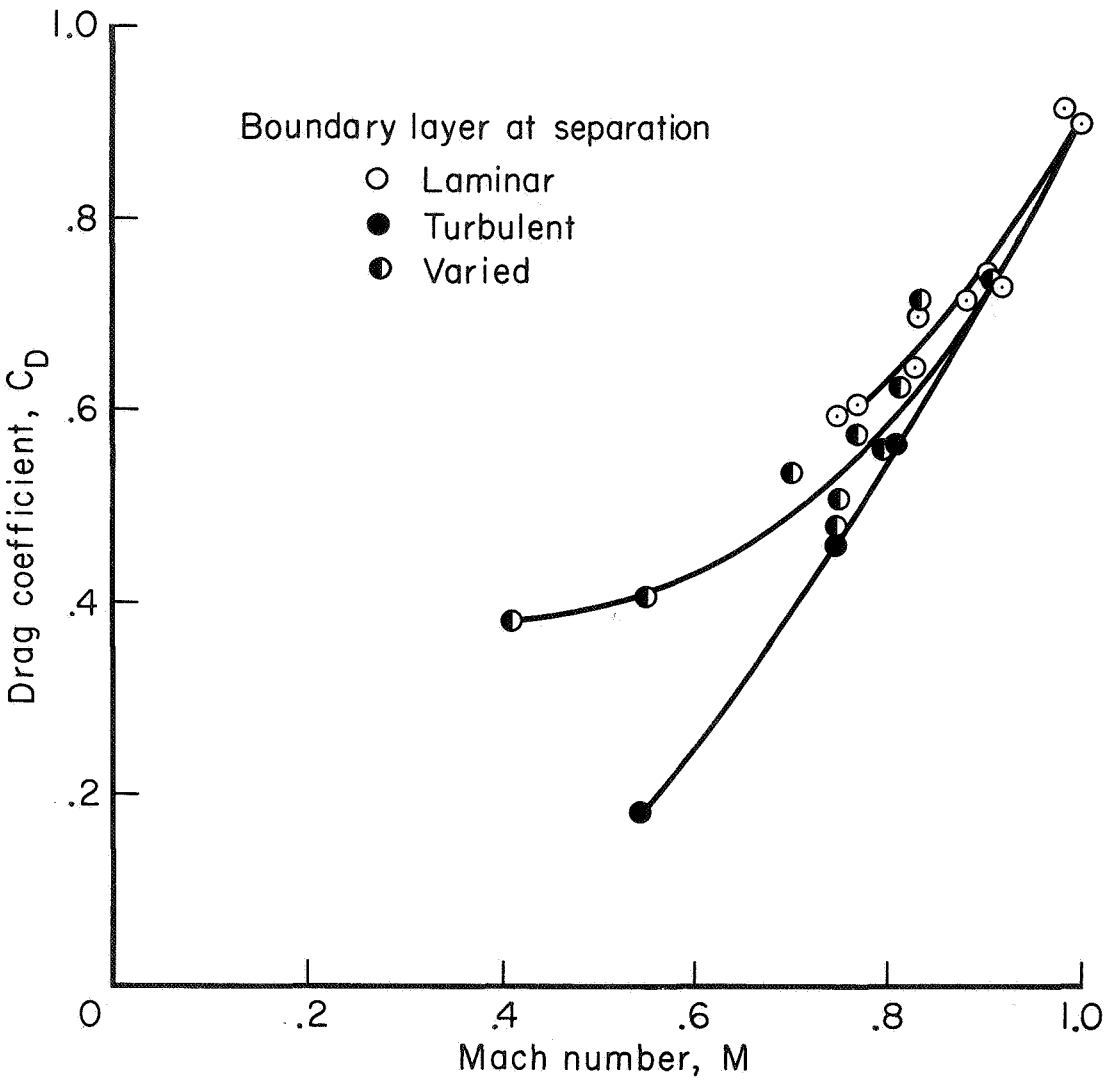

(b) Subsonic regime.

Figure 14.- Concluded.

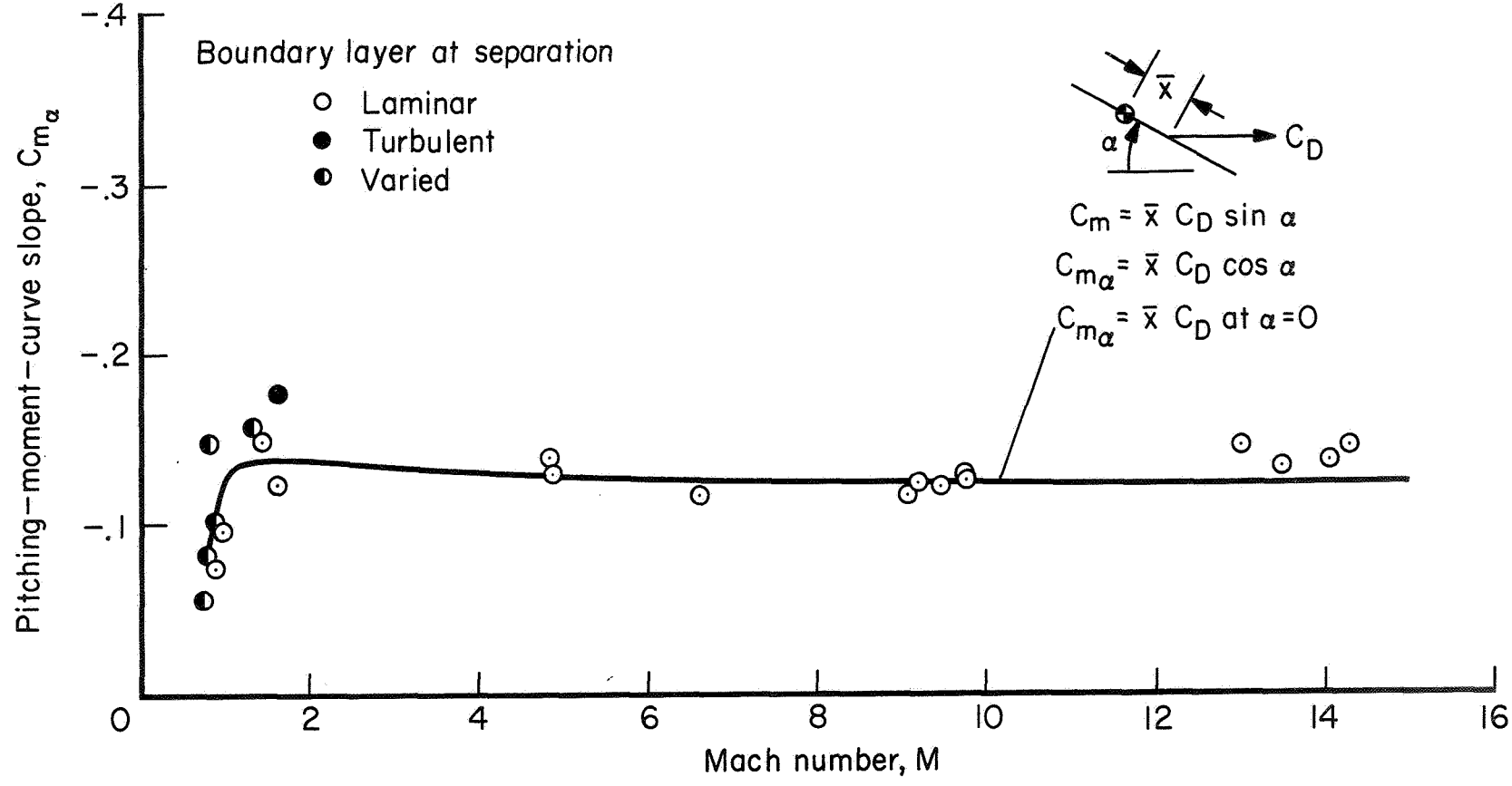

Figure 15.- Static-stability data.

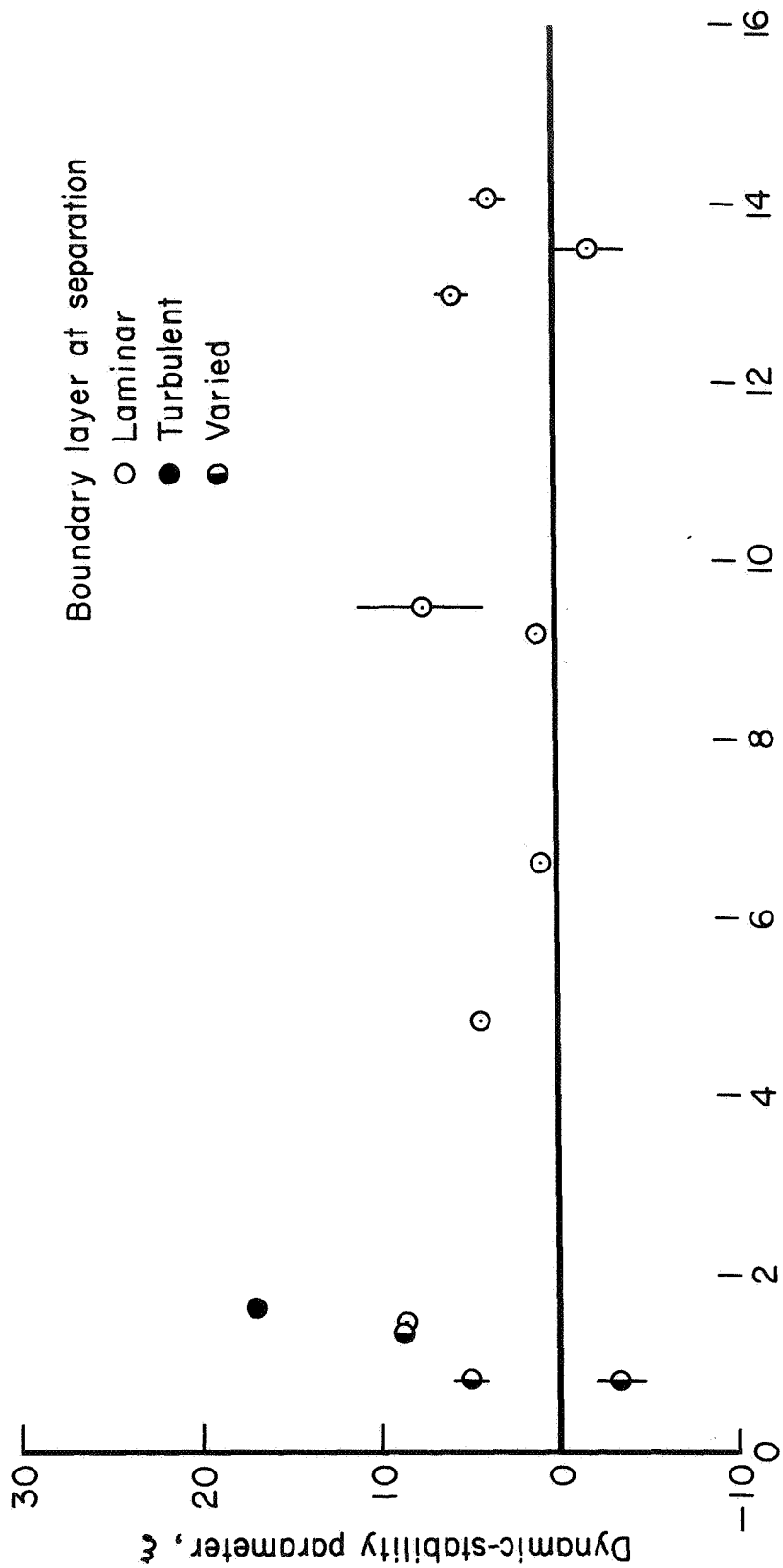

Figure 16.- Dynamic-stability data.

"The aeronautical and space activities of the United States shall be conducted so as to contribute . . . to the expansion of human knowledge of phenomena in the atmosphere and space. The Administration shall provide for the widest practicable and appropriate dissemination of information concerning its activities and the results thereof."

—NATIONAL AERONAUTICS AND SPACE ACT OF 1958

NASA SCIENTIFIC AND TECHNICAL PUBLICATIONS

TECHNICAL REPORTS: Scientific and technical information considered important, complete, and a lasting contribution to existing knowledge.

TECHNICAL NOTES: Information less broad in scope but nevertheless of importance as a contribution to existing knowledge.

TECHNICAL MEMORANDUMS: Information receiving limited distribution because of preliminary data, security classification, or other reasons.

CONTRACTOR REPORTS: Scientific and technical information generated under a NASA contract or grant and considered an important contribution to existing knowledge.

TECHNICAL TRANSLATIONS: Information published in a foreign language considered to merit NASA distribution in English.

SPECIAL PUBLICATIONS: Information derived from or of value to NASA activities. Publications include conference proceedings, monographs, data compilations, handbooks, sourcebooks, and special bibliographies.

TECHNOLOGY UTILIZATION PUBLICATIONS: Information on technology used by NASA that may be of particular interest in commercial and other non-aerospace applications. Publications include Tech Briefs, Technology Utilization Reports and Notes, and Technology Surveys.

Details on the availability of these publications may be obtained from:

SCIENTIFIC AND TECHNICAL INFORMATION DIVISION

NATIONAL AERONAUTICS AND SPACE ADMINISTRATION

Washington, D.C. 20546